Journal of Advances in Modeling Earth Systems

RESEARCH ARTICLE
10.1029/2017MS001044

Robust Inverse Modeling of Growing Season Net Ecosystem Exchange in a Mountainous Peatland: Influence of Distributional Assumptions on Estimated Parameters and Total Carbon Fluxes

Tobias K. D. Weber[1,2,3], Lars Gerling[4], Daniela Reineke[5], Stephan Weber[4], Wolfgang Durner[1], and Sascha C. Iden[1]

[1]Division of Soil Science and Soil Physics, Institute of Geoecology, Technische Universität Braunschweig, Braunschweig, Germany, [2]Now at Institute of Soil Science and Land Evaluation, University of Hohenheim, Stuttgart, Germany, [3]Department of Geography and Environmental Management, University of Waterloo, Waterloo, ON, Canada, [4]Division of Climatology and Environmental Meteorology, Institute of Geoecology, Technische Universität Braunschweig, Braunschweig, Germany, [5]Department of Plant Sciences, University of California, Davis, CA, USA

Key Points:
- Half-hourly CO_2 flux data from a peatland were used to calibrate a net ecosystem exchange (NEE) model using a robust MCMC sampler
- Robust inverse modelling accounted for non-Gaussian model errors and standardization by a vapor pressure deficit dependent weighting scheme
- Adoption of Student's t likelihood model led to different parameters, reduced uncertainties, and a difference in cumulative NEE

Supporting Information:
- Data Set S1

Correspondence to:
T. K. D. Weber,
tobias.weber@uni-hohenheim.de

Citation:
Weber, T. K. D., Gerling, L., Reineke, D., Weber, S., Durner, W., & Iden, S. C. (2018). Robust inverse modeling of growing season net ecosystem exchange in a mountainous peatland: Influence of distributional assumptions on estimated parameters and total carbon fluxes. *Journal of Advances in Modeling Earth Systems*, *10*, 1319–1336. https://doi.org/10.1029/2017MS001044

Received 5 DEC 2017
Accepted 6 APR 2018
Accepted article online 27 APR 2018
Published online 30 JUN 2018

Abstract While boreal lowland bogs have been extensively studied using the eddy-covariance (EC) technique, less knowledge exists on mountainous peatlands. Hence, half-hourly CO_2 fluxes of an ombrotrophic peat bog in the Harz Mountains, Germany, were measured with the EC technique during a growing season with exceptionally dry weather spells. A common biophysical process model for net ecosystem exchange was used to describe measured CO_2 fluxes and to fill data gaps. Model parameters and uncertainties were estimated by robust inverse modelling in a Bayesian framework using a population-based Markov Chain Monte Carlo sampler. The focus of this study was on the correct statistical description of error, i.e. the differences between the measured and simulated carbon fluxes, and the influence of distributional assumptions on parameter estimates, cumulative carbon fluxes, and uncertainties. We tested the Gaussian, Laplace, and Student's t distribution as error models. The t-distribution was identified as best error model by the deviance information criterion. Its use led to markedly different parameter estimates, a reduction of parameter uncertainty by about 40%, and, most importantly, to a 5% higher estimated cumulative CO_2 uptake as compared to the commonly assumed Gaussian error distribution. As open-path measurement systems have larger measurement error at high humidity, the standard deviation of the error was modeled as a function of measured vapor pressure deficit. Overall, this paper demonstrates the importance of critically assessing the influence of distributional assumptions on estimated model parameters and cumulative carbon fluxes between the land surface and the atmosphere.

1. Introduction

Peatlands cover only 3% of the land surface but store up to 30% of terrestrial carbon (Gorham, 1991). Carbon fluxes between peatland and atmosphere are strongly coupled to both the hydrological cycle and climatic conditions (e.g., Adkinson et al., 2011, Lindroth et al., 2007; Weber et al., 2017a). This gives rise to the assumption that local changes in rain patterns and an increase in temperature as predicted for central Europe (Hattermann et al., 2011) will affect the carbon fluxes in and out of peatlands. However, future changes of C sequestration in peatlands are difficult to predict, because meteorological conditions influence a variety of processes controlling the fate of C in peatlands (Gitay et al., 2001). Moreover, peatlands occur in different climate zones and differ in their physical and chemical properties, nutrient status, and vegetation; and thus, CO_2 exchange. While boreal lowland bogs have been extensively studied using the eddy-covariance (EC) technique, less knowledge exists on mountainous peatlands. To address this knowledge gap, we measured the CO_2 exchange of a temperate ombrotrophic peat bog in the Harz Mountains, Germany, during the very dry growing season of 2013.

EC is an established measurement technique to quantify the exchange of water and carbon between homogeneous and flat land surfaces and the lower atmosphere. With EC it is possible to directly and continuously measure atmospheric fluxes. For adequate turbulence conditions, measured fluxes have been shown to agree well with chamber measurements, also on sloped terrain (Hammerle et al., 2007). In northern peatlands, the

requirement of a homogeneous and flat surface is often met because of their extensive open surface area. As a consequence, there are numerous EC studies on exchange processes in preserved boreal peatlands (Kellner, 2001; Kurbatova et al., 2002; Moore et al., 2006; Runkle et al., 2014; Sutherland et al., 2014). In contrast, bogs in other climates and in particular undisturbed bogs, have been investigated less frequently. Despite the large number of small peatlands in mountain ranges (Pullens et al., 2016), there are only few EC studies conducted on these ecosystems as a result of their limited area and their complex local topography (Batzer & Baldwin, 2012). These site-specific characteristics may result in an influence of advection on measured fluxes (Etzold et al., 2010) and therefore possibly lead to temporary violations of the Monin-Obukhov similarity theory which is the basis for the EC flux calculation (Stiperski & Rotach, 2016) and in turn can lead to mixed flux signals for measurements in the transition layer (Nicolini et al., 2015). Nonetheless, previous studies successfully applied EC at sites with challenging turbulence characteristics (Heusinger & Weber, 2017; Weber & Kordowski, 2010). Furthermore, open path EC measurements are sensitive to low vapour pressure deficits because they lead to a contamination of the lenses of the infrared gas analyzer (IRGA; Serrano-Ortiz et al., 2008).

Models of net ecosystem exchange (*NEE*) have become essential tools in the micrometeorological analysis of vegetated sites. However, such models have to be calibrated to yield a robust filling of data gaps and reliable estimates of cumulative C uptake (Falge et al., 2001), to differentiate between respiration and photosynthesis, and to test our understanding of the underlying biophysical processes governing C exchange (e.g., Gilmanov et al., 2013; Lasslop et al., 2010; Raj et al., 2016). To achieve these goals, biophysical model parameters have to be estimated by inverse modeling using high-quality measured data sets. Central to the estimation of model parameters is the formulation of a statistical model of the differences between the model-predicted and observed system response. In the remainder of this article, we will refer to these difference as "errors". Under the assumption of negligible systematic errors, i.e. by assuming that the model is an unbiased representation of measured *NEE*, the remaining discrepancies between model and observations, caused by signal noise, unaccounted aspects of turbulent transport, varying footprint size or surface heterogeneity (Hollinger & Richardson, 2005; Moncrieff et al., 1996), are usually treated as random error. An adequate assumption about the statistical properties of the errors is crucial to correctly quantify true parameter and prediction uncertainty (Hollinger & Richardson, 2005). Most frequently, ordinary least squares (OLS) estimation has been used in peatland studies (e.g., Adkinson et al., 2011; Humphreys et al., 2006). OLS estimation assumes that the errors are mutually independent, normally distributed, have zero expectation, and equal variance (homoscedasticity). Under these assumptions, the parameters obtained from minimizing the OLS objective function can be regarded as maximum-likelihood estimates. For ecosystems other than peatlands, the validity of the statistical assumptions underlying OLS estimation has been questioned. More accurate calibration results in studies on forested sites have been achieved by introducing advanced weighting schemes to deal with variance heterogeneity (heteroscedasticity) (Lasslop et al., 2008) or by using non-Gaussian error distributions (Hollinger & Richardson, 2005; Richardson et al., 2008).

In this study, EC measurements over a mountainous, undisturbed bog in Central Europe were used to quantify *NEE*. An established biophysical model was calibrated to assess the dependence of *NEE* on photosynthetic active radiation and meteorological variables. We hypothesize that a Gaussian error distribution has to be rigorously tested as the actual differences between the calibrated model and the observations (residuals) may indeed be non-Gaussian. Model calibration and uncertainty quantification were carried out in a Bayesian framework using a population-based Markov-chain Monte Carlo (MCMC) algorithm. Besides the determination of maximum-likelihood estimates, we robustly quantified the posterior statistical distribution of the model parameters and the posterior predictive distribution of *NEE*. In the following, we test the performance of three likelihood functions which are based on different assumptions regarding the statistical error distribution. The influence of the distributional assumptions on i) the estimated model parameters, ii) biophysical response functions, and iii) *NEE* predictions, including cumulative *NEE* are analyzed, and the most adequate error model is identified by model performance criteria and an analysis of residuals. To describe heteroscedasticity, we introduce a model which relates the error standard deviation to the vapor pressure deficit and test its adequacy.

2. Material and Methods

2.1. Site Description and Instrumentation

During the growing season 2013, EC measurements were carried out over a 150 day time period from 5 June to 30 October at a soli-ombrotrophic peat bog site Odersprungmoor (OM), Harz Mountains, Central

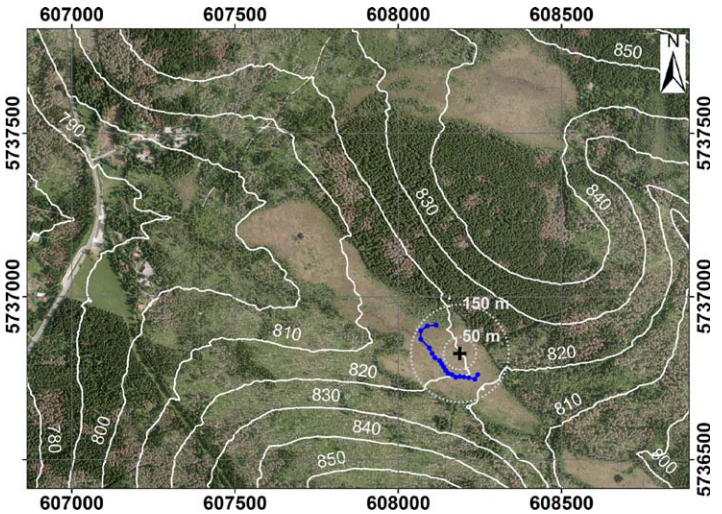

Figure 1. Aerial map of the study site with elevation contour lines (in m) (Surveying and Cadastral Authority Lower-Saxony, © 2015). The position of the EC-tower is denoted by the black cross. Blue dots indicate the average distance of the 90% footprint area for different wind directions in increments of 10 degrees within the accepted wind sector.

Germany (UTM 32U 608000 mE 5737000 mN; 800–821 m a.s.l.) The long-term average temperature is 6.8°C and annual precipitation is 1,270 mm. The bog has an open area of 16.9 ha which is surrounded by spruce forest and a vegetation height of less 20 cm. Further extensive vegetation mapping was carried out by Baumann (2009). The open part is almost elliptical in shape with the longer axes oriented in SE-NW direction and situated on a saddle with an average slope of 3% (Jensen, 1990). For the OM, Weber et al. (2017a, 2017b) show the complexity of soil hydraulic properties and their depth-dependence which exert an influence on gas fluxes in the soil and evaporation rates. The location of the site is illustrated in Figure 1. The months June and August, were the driest on a 100 year record on precipitation at nearby Braunlage, and due to the large amounts of precipitation in late July, the month was at the median precipitation amount. This is important, since extreme dry conditions can potentially lead to a net CO_2 release due to the oxidation of the organic soils in peatlands, and in particular peat bogs. All in all, the growing season of 2013 can be characterized to be, comparatively, very dry.

Three-dimensional wind components were measured with a sonic anemometer (CSAT3a; Campbell Scientific, Inc.) and water and CO_2 concentrations were measured with an open-path IRGA (EC150; Campbell Scientific, Inc. Logan, Utah, USA). The instruments were installed on a tower at 2 m height and orientated towards 232°. Both instruments measured at a frequency of 10 Hz. Furthermore, air temperature (T_a) and humidity were recorded by a HUMI-CAP HP155 (Vaisala Oyj, Helsinki, Finland), and incoming and outgoing short and longwave radiation with a net radiometer (NR01; Hukseflux Thermal Sensors B.V., Delft, Netherlands). The precipitation at the site was registered with a rain gauge (Theodor Friedrichs & Co. GmbH, Schenefeld, Germany). A mean soil temperature (T_s) of the upper soil layer was determined from measurements at 2 and 6 cm depth in the vicinity of the tower using thermocouple elements (TCAV-L; Campbell Scientific, Inc.). The volumetric soil water content was monitored at 4 cm depth by a moisture probe (CS616L; Campbell Scientific, Inc.). The groundwater table depth was monitored from 29 June onwards with a tensiometer (T5 Tensiometers, UMS, Munich, Germany) in 60 cm depth.

2.2. Data Processing

Raw EC data were processed with the EddyPro v6.2.0 software (LI-COR Biosciences Inc., 2014) to obtain half-hourly fluxes. Fluxes occurring at wind directions (ϕ) between 320 and 135° were discarded due to the proximity to the surrounding forest and hillslope (compare Figure 1). The footprint was calculated according to the model by Kljun et al. (2004), if the atmospheric stability parameter ζ was within $-200 < \zeta < 1$ and the friction velocity u^* was greater than 0.2 m s^{-1}. In cases where these necessary conditions were not met, the footprint was calculated by the model of Kormann and Meixner (2001). Half-hourly fluxes of CO_2 were computed from measured and corrected variables by the equation

$$F_{CO_2} = \overline{w' \rho'_{CO_2}} \quad (1)$$

where F_{CO_2} is the measured flux density of carbon dioxide (μmol s^{-1} m^{-2}), w is the vertical wind speed (m s^{-1}), and ρ_{CO2} is the concentration of CO_2 in dry air (μmol m^{-3}). The apostrophe in equation (1) denotes the fluctuating term and the overbar indicates the mean within the averaging period. F_{CO2} is a measure for *NEE* and used synonymously in EC studies (e.g., Adkinson et al., 2011; Lafleur et al., 2001). Data were discarded (i) if the turbulence and steady state criterion by Foken (2006) was >7, (ii) under low turbulence conditions at nighttime, (iii) if they fell outside the footprint length of 1,000 m, (iv) if the IRGA signal strength < 70%, and (v) during precipitation events. This led to a data availability limited to 34% of the measurement period, a similar value for mountainous peatlands was found by Pullens et al. (2016). The reason was mainly because of dew formation on the sensor of the IRGA and inadequate turbulence conditions. For the accepted data, the mean 90% footprint of the data set was within the outer boundaries of the peat bog which guarantees that the measured *NEE* is representative of the bog and undisturbed by the surrounding forest.

The groundwater table depth was calculated from the tensiometer data by assuming hydrostatic conditions, i.e. a linear pressure head distribution with depths. The pressure head measured with the tensiometer (60 cm depth) was positive throughout the entire measurement period indicating that the water table depth did not fall under the installation depth. This indicates that the profile was well-watered throughout the measurement campaign. As a consequence, neither the effect of water table depth nor volumetric water content were included in the model for *NEE*. We checked this assumption a posteriori by analyzing the relationship between the residuals and volumetric water content.

2.3. Model for NEE

NEE (μmol m^{-2} s^{-1}) was described as the sum of gross primary production *GPP* (μmol m^{-2} s^{-1}) and ecosystem respiration *ER* (μmol m^{-2} s^{-1})

$$NEE = ER + GPP \tag{2}$$

We follow the sign convention that a flux directed from the surface to the atmosphere gets a positive sign and vice versa. As a result, a positive *NEE* indicates a net CO_2 release from the bog and a negative *NEE* indicates an uptake of CO_2 by net photosynthesis.

The *ER* flux was modelled with van't Hoff's Q_{10} model (Van't Hoff, 1898). This model is often used to describe temperature dependent ecosystem respiration at peatland locations (Adkinson et al., 2011; Glenn et al., 2006; Parmentier et al., 2009) and is given by

$$ER = BR \cdot Q_{10}^{\frac{T_s - T_{ref}}{T_{ref}}} \tag{3}$$

where *BR* is the base rate respiration at 10°C (μmol m^{-2} s^{-1}), Q_{10} is a parameter describing temperature sensitivity, T_s is the soil temperature which is assumed to control respiration rates (°C), and $T_{ref} = 10°C$ is the reference temperature.

In accordance with other peatland studies such as Bubier et al. (2002), Glenn et al. (2006), Adkinson et al. (2011), and Campbell et al. (2014), *GPP* was modelled assuming a hyperbolic light response curve (Tamiya, 1951; Zobitz et al., 2011). Here, we additionally account for a temperature dependence of the light-use efficiency *LUE* (Yuan et al., 2007) so that the model for *GPP* is

$$GPP = -A_{\max} \cdot \frac{Q_{PPFD} \cdot LUE(T_a)}{A_{\max} + Q_{PPFD} \cdot LUE(T_a)} \tag{4}$$

where $A_{\max}$ is the maximum assimilation rate of CO_2 (μmol m^{-2} s^{-1}), Q_{PPFD} (μmol m^{-2} s^{-1}) is the photosynthetically active photon flux density, and $LUE(T_a)$ is given in (μmol CO_2 (μmol PPFD)$^{-1}$). The temperature response of the light use efficiency is parameterized by the equation

$$LUE(T_a) = \begin{cases} L_{\max} \dfrac{(T_a - T_{\min}) \cdot (T_a - T_{\max})}{(T_a - T_{\min}) \cdot (T_a - T_{\max}) - (T_a - T_{\text{opt}})^2} & \text{if } T_{\min} < T_a < T_{\max} \\ 0 & \text{otherwise} \end{cases} \tag{5}$$

where T_{min} and T_{max} are the minimum and maximum air temperatures for photosynthesis (°C), respectively, and T_{opt} is the optimal temperature (°C) at which $LUE(T_a)$ equals L_{max}, which is the maximum light use efficiency (μmol CO_2 (μmol PPFD)$^{-1}$) (Yuan et al., 2007). The influence of water content on NEE is not considered. Throughout this study, T_{min} and T_{max} were set to 0 and 40°C, respectively, and T_{opt} was estimated by inverse modeling. The photosynthetically active photon flux density Q_{PPFD} (μmol m^{-2} s^{-1}) was estimated from incoming short wave radiation ($K\downarrow$) by assuming that approx. 50% of $K\downarrow$ is photosynthetically active (Szeicz, 1974) and 1 W m^{-2} equals 4.2 μmol m^{-2} s^{-1} of Q_{PPFD} (McCree, 1972). This biophysical model is not dependent on the ambient CO_2 concentration which can be ignored for studies covering only a few years and less.

2.4. Parameter Estimation and Uncertainty Analysis

The observed *NEE* data were used to identify the values of the model parameters *BR*, Q_{10}, $A_{\max}$, $L_{\max}$, and T_{opt} by inverse modeling. Parameter estimation was carried out in a Bayesian framework, i.e. the unknown model parameters were treated as random variables. The joint probability density function (pdf) of the

model parameters was approximated by Markov Chain Monte Carlo (MCMC) sampling, a technique which generates a representative sample from the parameter pdf (Brooks, 1998).

According to the continuous case of Bayes' theorem, the posterior pdf of the model parameters is (Box & Tiao, 1992; Reichert & Omlin, 1997)

$$f_{\text{post}}(\boldsymbol{p}|\boldsymbol{y}) = \frac{L(\boldsymbol{y}|\boldsymbol{p}) f_{\text{prior}}(\boldsymbol{p})}{f(\boldsymbol{y})} \tag{6}$$

where $f_{\text{post}}(\boldsymbol{p}|\boldsymbol{y})$ is the posterior distribution of the model parameters $\boldsymbol{p}$, conditional on the time series vector of observed *NEE* fluxes, denoted by $\boldsymbol{y}$, $L(\boldsymbol{y}|\boldsymbol{p})$ is the likelihood function, $f_{\text{prior}}(\boldsymbol{p})$ is the prior distribution of the model parameters, and $f(\boldsymbol{y})$ is the probability density of the measurements, or evidence. As $f(\boldsymbol{y})$ is independent of the model parameters, it serves as a normalizing constant which ensures that $f_{\text{post}}(\boldsymbol{p}|\boldsymbol{y})$ integrates to unity. By assuming a non-informative prior distribution, i.e. a uniform distribution within physically feasible parameter bounds, the posterior becomes proportional to the likelihood function within the parameter bounds. As posterior sampling by MCMC requires that $f_{\text{post}}(\boldsymbol{p}|\boldsymbol{y})$ is only known up to a constant of proportionality (Gelman et al., 2004), MCMC sampling is possible without specifying $f(\boldsymbol{y})$. More information on the interpretation of the different pdfs can be obtained from standard textbooks like Box and Tiao (1992) and Gelman et al. (2004).

By assuming statistically independent observations $\boldsymbol{y}$, the likelihood function can be written as the product of N individual likelihoods L_i which quantify the probability to observe a single data point y_i

$$L(\boldsymbol{y}|\boldsymbol{p}) = \prod_{i=1}^{N} L_i(y_i|\boldsymbol{p}) \tag{7}$$

In the following, we present the mathematical expressions for the individual likelihood functions L_i for different assumptions regarding the error, i.e. the difference between model-predicted and observed *NEE* fluxes. The error is defined as

$$e_i(\boldsymbol{p}) = y_i - f(t_i, \boldsymbol{p}) \; i = 1, \ldots, N \tag{8}$$

where $f(t_i, \boldsymbol{p})$ denotes the model-predicted flux at time t_i. Throughout this study, the errors are assumed to have an expectation of zero, and are normalized by their standard deviation σ_i (μmol s^{-1} m^{-2}) to yield a standardized error

$$\underline{e}_i(\boldsymbol{p}) = \frac{e_i}{\sigma_i} \;\; i = 1, \ldots, N \tag{9}$$

The fact that the standard deviation of the error σ_i can vary with the magnitude of the observed variable has been acknowledged in CO_2 forest-atmosphere exchange studies, too (e.g., Van Wijk et al., 2008). As open path EC measurements are rather sensitive to air humidity due to a possible contamination of the lenses of the IRGA (Serrano-Ortiz et al., 2008), measurement error is expected to be higher when the water vapor pressure deficit is small. The relationship between σ and the vapor pressure deficit D_v (kPa) was modelled by the smoothed piecewise linear function (Chen & Mangasarian, 1996; Iden & Durner, 2014)

$$\sigma(D_v) = \sigma_1 + \frac{\sigma_2 - \sigma_1}{D_{vc}} \left\{ D_{vc} - D_v + m \ln \left[1 + \exp\left(\frac{D_v - D_{vc}}{m} \right) \right] \right\} \tag{10}$$

where σ_1 (μmol s^{-1} m^{-2}), σ_2 (μmol s^{-1} m^{-2}), and D_{vc} (kPa) are model parameters and m=0.01 kPa is a parameter which smoothes the function $\sigma(D_v)$ around D_{vc}. Equation (10) predicts a linear decrease of σ from σ_2 to σ_1 within the interval $0 < D_v < D_{vc}$ and a constant value of σ_1 for $D_v > D_{vc}$. The standard deviation of the error in *NEE* was calculated as function of D_v by equation (10) and then used to standardize the residuals by equation (9).

Under the assumptions that the standardized residuals follow a Gaussian distribution with expectation zero, the probability to observe a single data point y_i is (Aster et al., 2013)

$$L_i(y_i|\boldsymbol{p}) = \frac{1}{\sqrt{2\pi}\sigma_i} \exp\left(-0.5 \; \underline{e}_i^2\right) \tag{11}$$

and the likelihood function is calculated by the product defined by equation (7).

Hollinger and Richardson (2005) proposed a Laplace distribution to describe a more heavily-tailed distribution of the error with a pronounced peak. Assuming a Laplace-distribution with expected value zero, the likelihood to observe a single data point is

$$L_i(y_i|\boldsymbol{p}) = \frac{1}{\sqrt{2}\ \sigma_i} \exp\left(-\sqrt{2}\,|\underline{e}_i|\right) \tag{12}$$

The third model to describe the statistical distribution of the residuals in this article is Student's *t*-distribution (Aster et al., 2013). The t-distribution is symmetric around its expected value of zero and has heavier tails than the Gaussian distribution (Lange et al., 1989). The likelihood to observe a single data point assuming the t-distribution is (Scharnagl et al., 2015)

$$L_i(y_i|\boldsymbol{p}) = \frac{\Gamma\left(\frac{\nu+1}{2}\right)}{\sqrt{\nu\ \pi}\ \Gamma\left(\frac{\nu}{2}\right)\sigma_i} \left(1+\frac{e_i^2}{\nu}\right)^{-\frac{\nu+1}{2}} \tag{13}$$

where Γ denotes the gamma function and ν is a kurtosis parameter which is constrained to values greater than two. The advantage of the t-distribution over the Laplace distribution is that it is less peaked, rounder in the vicinity of the mode, and that it converges to a normal distribution for $\nu \to \infty$. The variance of the t-distribution is $\nu/(\nu-2)$ and for small values of ν it produces increasingly heavier tails compared to the normal distribution. As the value of ν is not known a priori, ν was estimated as an additional parameter. As a consequence, the total number of estimated parameters is 8 for the Gauss and Laplace distributions (5 parameters for the *NEE* model, 3 nuisance parameters to describe heteroscedasticity) and 9 for the t-distribution (ν as additional nuisance parameter). Note that the error standard deviation σ_i occurs in the denominator of equation (13) to ensure that the pdf integrates to unity after standardizing the error by its standard deviation.

The posterior distribution of the estimated model parameters was estimated by MCMC sampling using the population-based MCMC sampler DREAM (DiffeRential Evolution Adaptive Metropolis; Vrugt et al., 2009). A technical summary of the algorithm, recommendations for use, details on convergence diagnostics, and example applications are presented in Vrugt (2016). We used the *dream* package (Guillaume & Andrews, 2012; Joseph & Guillaume, 2013) in R (R Core Team, 2015). The control parameters for the DREAM algorithm are summarized in Table 1. As mentioned, a uniform prior distribution within physical viable parameter bounds (Table 2) was used. The final number of parameter sets used for statistical inference after thinning was 10,000. The three models of the likelihood function were compared using the maximum value of the log-posterior $log\, f_{post}(\hat{\boldsymbol{p}}|\boldsymbol{y})$, where $\hat{\boldsymbol{p}}$ is the mode of the posterior, and the deviance information criterion DIC (Spiegelhalter et al., 2002) defined as

Table 1
Control Parameters Used in the DREAM Algorithm

Parameter	Explanation	Value/option
ndim	Number of parameters to be estimated	8 (normal/Laplace) 9 (t)
DEpairs	Number of pairs to generate a jump	3
nCR	Number of crossover values	3
Steps	Number of steps used for the adaptive tuning of crossover values	10
gamma	Kurtosis parameter of the Bayesian Inference Scheme	0
eps	Random error of ergodicity	0.001
outliertest	Test for outliers within a chain	IQR test
thin.t	Chain thinning for the resulting samples	10
boundHandling	Method to handle constraint violations	Reflection
burnin.length	Portion of data discarded to avoid burn-in effects	0.7
ndraw	Maximum number of generated samples	200,000
Rthres	Threshold for Gelman-Rubin statistic	1.1

Note. The parameter names are the option names as used in the R implementation of the algorithm (Guillaume & Andrews, 2012). Further explanation on the parameters is given by Vrugt (2016)

Table 2
Lower and Upper Bounds Used to Define the Uniform Prior Distribution of the Estimated Model Parameters

Parameter	*BR*	Q_{10}	A_{max}	L_{max}	T_{opt}
Units	(μmol m^{-2} s^{-1})		(μmol m^{-2} s^{-1})		(°C)
Lower bound	0	0	15	0	5
Upper bound	6	5	25	1	15

$$DIC = D(\hat{\boldsymbol{p}}) + 2n_D \quad (14)$$

where the deviance D is defined as twice the negative log posterior, and n_D is the Bayesian complexity or effective number of model parameters which is defined as (Spiegelhalter et al., 2002)

$$n_D = \overline{D(\boldsymbol{p})} - D(\bar{\boldsymbol{p}}) \quad (15)$$

where the overbar indicates the mean. In Bayesian model selection, the DIC allows a direct comparison of models with different number of parameters and the model with the smallest DIC is favored over the other models.

The uncertainty of the estimated model parameters was assessed by a statistical analysis of the generated parameter sample. We calculated the mode, median, variance, coefficient of variation (CV, standard deviation divided by the mode), 2.5% and 97.5% quantiles, and 95% interquantile range (IQR). The uncertainty of the model prediction caused by the uncertainty in the parameters was assessed by propagating the parameter samples through the *NEE* model and calculating the 95%-IQR of the model prediction. Prediction uncertainty was quantified by drawing samples from the posterior predictive distribution as described in Gelman et al. (2004) and Iden and Durner (2008). The uncertainty of the estimated nuisance parameters was accounted for.

3. Results and Discussion

3.1. Measured Environmental Variables

An overview of meteorological and hydrological conditions and their seasonal variation during the measurement period is given in Figure 2. Daily means of $K\downarrow$, T_a and T_s were highest during July and decreased towards fall. The vapor pressure deficit was generally low throughout the measurement period with a mean RH in July of 78% and 91% in September and October. The soil water content was lowest in July and increased towards the fall, which coincides with the daily sums of precipitation, which were low in July and August, and very high in September and October. Although there was a higher precipitation sum in July than in August, the volumetric water content of the soil declined to 0.4 due to a period of 19 consecutive days without rain (Figure 2). The measured evapotranspiration was very close to the potential evapotranspiration as calculated with the Penman-Monteith equation assuming a surface resistance of zero; and thus, depended mainly on meteorological conditions and was unaffected even by the low volumetric water contents as a potential limitation to water availability (data not shown). Figure 2 shows a large variability in meteorological drivers and volumetric soil moisture conditions.

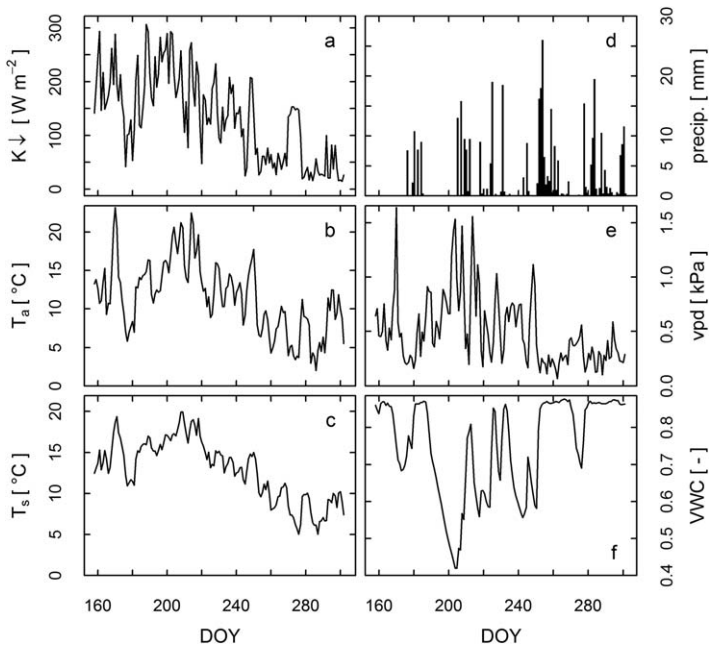

Figure 2. Daily means of (a) incoming shortwave radiation, (b) air temperature, (c) soil temperature, (d) daily sum of precipitation, (e) vapor pressure deficit(vpd), and (f) half hourly volumetric water contents (VWC). Precipitation is not available before DOY 180.

Midday median F_{CO2} in July and August were highest with up to −11 μmol m^{-2} s^{-1}. In September, the measured midday median flux density was −8 μmol m^{-2} s^{-1} and in October it was −4 μmol m^{-2} s^{-1}. Despite the relatively dry conditions in July, no reduction in observed CO_2 uptake by the studied peat bog could be related to low volumetric moisture content or water table depth. Following a typical seasonal trend, daily means of observed carbon fluxes were highest in July with −3.1 g C m^{-2} d^{-1}. Midday F_{CO2} in August is similar to midday F_{CO2} in July while higher respiration rates at night occurred in August leading to an average daily F_{CO2} of −2.0 g C m^{-2} d^{-1}. In September and October, shorter day lengths and reduced $K\downarrow$ led to a limitation of *GPP* causing a further reduction in net uptake in September (-1.1 g C m^{-2} d^{-1}) and a net loss in October (0.4 g C m^{-2} d^{-1}). Median diurnal variations for the different months and the entire campaign are presented at the end of the manuscript together with the simulation results.

Table 3
Comparison of the Performance of the Three Likelihood Models: Mean Weighted Error, Log Posterior Likelihood, and Deviance Information Criterion (DIC)

Likelihood model	Mean weighted error	Log-posterior	DIC
Normal	−0.003	−6,066	12,147
Laplace	−0.03	−5,564	11,143
Student's t	−0.09	−5,506	11,030

3.2. Comparison of Statistical Models

Table 3 summarizes the maximum log-posterior-likelihood and the DIC for the three different statistical models compared in this study. The model calibration which is based on the t-distribution has the highest posterior likelihood and the smallest DIC and is therefore identified as the best model. The improvement obtained by switching from the Gaussian to the Laplace distribution is more pronounced than that obtained from switching from the Laplace to the t-distribution. Obviously, a statistical error distribution with heavier tails is needed for modeling the data set with the applied *NEE* model. Note that the higher number of estimated parameters in case of the t-distribution (9 compared to 8) is accounted for in the DIC.

The fact that the t-distribution is best suited to describe the data is confirmed by the analysis of residuals in Figure 3. On the left-hand side histograms of the standardized model residuals, $\underline{e}_i$, together with the corresponding theoretical pdfs are shown (standard normal, standard Laplace, t-distribution). On the right-hand side, quantile-quantile plots are shown which compare the empirical quantiles of the standardized residuals with their theoretical equivalents. It becomes evident that neither the Gauss nor the Laplace distributions can describe the heavy tails of the distribution while the quantile-quantile for the t-distribution indicates an excellent agreement between the pdf and the residuals. This shows that the standardized residuals closely follow the t-distribution.

Figure 4 shows additional diagnostic plots for the model using the t-distribution. The top-left plot (a) shows the estimated relationship between the error standard deviation and the vapor pressure deficit defined by equation (10). The grey-shaded area symbolizes the 95%-IQR. The estimated standard deviation (posterior mode) decreases from 6.5 μmol m^{-2} s^{-1} at a D_v of 0 kPa and approaches 1.5 μmol m^{-2} s^{-1} in the vicinity of D_{vc} which was estimated to be 0.16 kPa. The shape of the function suggests that the error standard deviation decreases until a critical value of D_v is reached, above which the IRGA measures the CO_2 flux with an approximately constant precision (see Billesbach, 2011). This demonstrates that the assumption of a higher measurement error for small vapor pressure deficits is nicely reflected in the data and correctly identified by inverse modeling. We hypothesize that the model of the standard deviation given by equation (10) is generalizable to other studies using open path systems in settings with high relative humidity.

The time series of the standardized residuals shown in Figure 4b (top-right) indicates that the identified model for the dependence of the error standard deviation on the D_v leads to variance homogeneity (homoscedasticity) of the standardized residuals and is thus correct. Moreover, no seasonal trend is visible in the time series of the standardize residuals. The importance of this is discussed in detail in section 3.4. In the center-right plot (Figure 4d), the standardized residuals are plotted versus the modelled *NEE* to highlight that the model is adequate for both negative and positive values of the *NEE*. Figure 4d confirms this by illustrating that the error has a homogeneous variance and zero bias. Thus, the model for the *NEE* and the error model are adequate both for positive *NEE* (daytime, dominant GPP) and negative *NEE* (nighttime, ER).

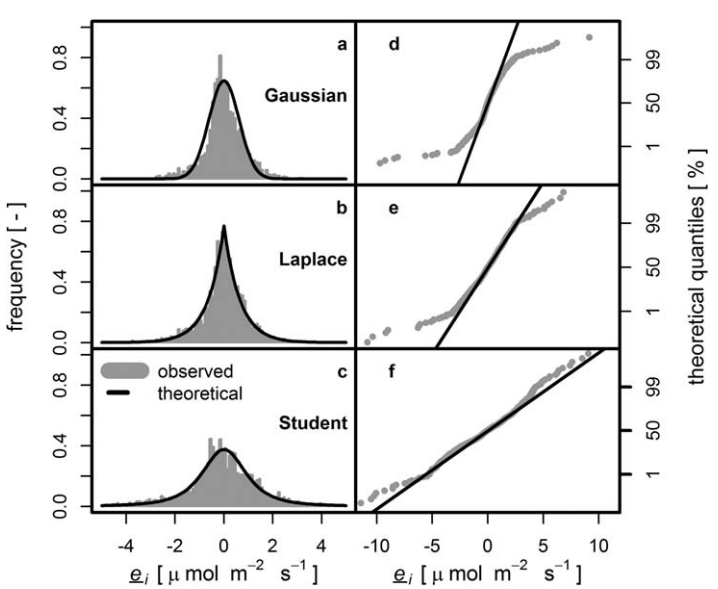

Figure 3. (a-c) Histograms and (d-f) quantile-quantile plots of standardized residuals for the normal (a and d), Laplace (b and e) and t-distribution (c and f).

The empirical autocorrelation function of the standardized residuals indicates a minor degree of autocorrelation and supports the assumption of independent errors made in equation (7) (Figure 4c, center-left). This is particularly noteworthy, as the simulations are based on half hourly measurements. This also implies that it is not required to include vegetation senescence in the applied *NEE* model for the fall measurements, because seasonal trends in photosynthesis and respiration are not observable. This might be due to the very long vegetation period at the site (April-November) and because our measurements did not cover the vegetation growth in spring.

Finally, Figure 4e (bottom right) shows that the standardized residuals do not show any discernible correlation with the water content in the top peat layer, i.e. their binned mean (black dots) and variance (scatter of grey dots) are almost independent of the water content. The only

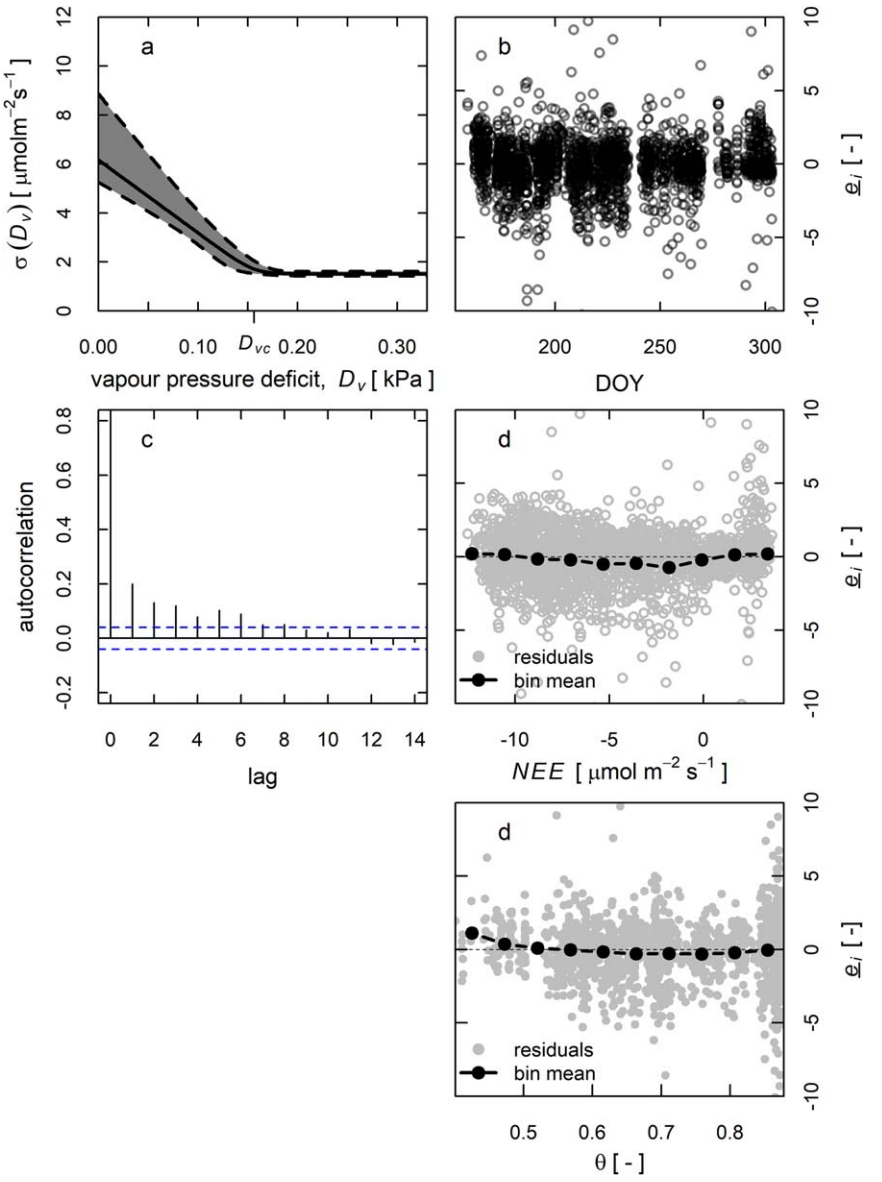

Figure 4. Analyses of the standardized residuals for the inference based on the t-distribution. Relationship between standard deviation and the VPD including 95 % estimation uncertaity (a), (b) time series of the standardized residuals, (c) empirical autocorrelation function, (d) standardized residuals versus the fitted NEE, and (e) standardized residuals as function of the water content in the top peat layer including the bin mean.

exception is under the driest condition with a moisture content of < 0.45 were the mean exceeds the null line by 1.5 µmol m^{-2} s^{-1}. However, there are only very few measurements available in this range ($< 0.2\%$ of the data set) and the mean of the second driest bin is already only marginally different from zero. Overall, this supports our model choice which neglects the effect of water table depth or soil water content on *NEE* in the model, although its influence on NEE in ombrotrophic peatlands has been acknowledged (e.g., Brown et al., 2017; Lund et al., 2007; Strachan et al., 2016). Different approaches exist to modify biophysical models by explicitly accounting for water table depth (Strack & Zuback, 2013; Strack et al., 2014). Given the results shown in Figure 4, we conclude that in spite of the exceptionally dry weather spells, the effect of water content on *NEE* can be neglected in this study.

3.3. Model Parameters, Response Functions and Uncertainties

The mode and median of the estimated model parameters are shown in Table 4 together with their 95%-IQR_{par} and the coefficient of variation (CV). In general, the mode deviated only slightly from the mean for all

Table 4
Estimated Parameters (Mode of the Posterior), Median Parameter Values, 2.5% and 97.5% Quantiles, and Coefficient of Variation (CV) for the NEE Model Parameters and the Three Error Models Compared in This Study

Parameter	BR	Q_{10}	A_{max}	L_{max}	T_{opt}	σ_2	σ_1	D_{vc}	ν
Units	(μmol m^{-2} s^{-1})		(μmol m^{-2} s^{-1})		(°C)	(μmol m^{-2} s^{-1})	(μmol m^{-2} s^{-1})	(kPa)	
				Normal Distribution					
Median	2.86	1.28	20.03	0.038	8.12	2.8	15.6	0.22	*na*
Mode	2.93	1.31	19.38	0.043	8.02	2.8	16.4	0.22	*na*
2.5%	2.65	1.14	18.74	0.038	5.2	2.7	14.5	0.21	*na*
97.5%	3.13	1.43	20.67	0.047	9.7	2.9	18.9	0.23	*na*
CV	4.3%	6.0%	2.5%	5.6%	14.2%	1.6%	7.2%	1.8%	*na*
				Laplace Distribution					
Median	2.31	1.74	20.8	0.034	11.6	2.6	12.9	0.16	*na*
Mode	2.33	1.72	20.8	0.033	11.3	2.5	12.2	0.19	*na*
2.5%	2.22	1.53	19.96	0.031	9.05	2.5	10.3	0.16	*na*
97.5%	2.44	1.81	22.05	0.036	12.14	2.7	15.8	0.20	*na*
CV	2.6%	4.2%	2.5%	3.2%	8.3%	2.1%	10.9%	6.6%	*na*
				Student's t Distribution					
Median	2.45	1.49	20.74	0.034	9.1	1.6	7.9	0.15	2.7
Mode	2.50	1.52	20.83	0.034	9.3	1.5	6.5	0.16	2.3
2.5%	2.32	1.42	19.99	0.032	8.5	1.4	5.2	0.13	2.1
97.5%	2.56	1.67	21.80	0.036	11.2	1.6	8.9	0.17	2.7
CV	2.4%	4.2%	2.2%	2.9%	7.8%	2.9%	11.8%	7.5%	5.5%

estimated parameters, indicating that the posterior parameter distributions were minimally skewed. The assumption of a normal distribution resulted in differences estimates of the parameters BR, Q_{10}, T_{opt}, and L_{max} compared to the other two distribution assumptions. More strikingly, in the majority of cases even the 95%-IQR$_{par}$ ranges do not overlap with those obtained for either the Laplace or t-distributions. The estimated BR and L_{max} obtained with the normal distribution assumption were smaller, and the values of Q_{10}, A_{max} and T_{opt} were higher than those estimated using the non-Gaussian distributions. The estimated biophysical model parameters were similar for the Laplace and t-distributions. The uncertainty of the estimated parameters (95%-IQR$_{par}$ and CV) reveals a reduction in uncertainty when switching from the Gauss- to the Laplace-distribution. The smallest CV values of the biophysical model parameters were obtained using the t-distribution. All values are smaller than 5% except for parameter T_{opt} with a relative estimation uncertainty of approx. 8%. These results show that parameter uncertainty is reduced if the errors are described using heavier tailed distributions, while in the case of the Gauss distribution undue weight is given to residuals located further away from zero (Finsterle & Najita, 1998; Hollinger & Richardson, 2005).

These findings are corroborated by the pairwise scatter plots and histograms shown in Figure 5 which visualize the parameter sample drawn from the posterior pdf using the DREAM algorithm in case of the t-distribution. Note that the parameter samples show a large distance from the bounds of the prior distribution given in Tab. 2, indicating a complete sampling of the parameter space. All correlation coefficients indicate a small to moderate cross-correlation between the model parameters. The parameters for the maximal assimilation rate A_{max} and the maximum light use efficiency L_{max} show a negative correlation but the value of -0.71 is still moderate. For biophysical reasons, a correlation between T_{opt} and Q_{10} must also be expected, but the correlation coefficient is only 0.64. These small values also prove that all parameters were identifiable. For future studies, these indices can be used to construct informative prior distributions for a Bayesian inference scheme.

The determined parameters in the model for heteroscedasticity in equation (10) are comparable for the Gauss and Laplace distributions. In contrast to this, the two standard deviations σ_1 and σ_2 are much smaller for the t-distribution. These small values are compensated by the additional dispersion of the t-distribution, i.e. the estimated value of ν was 2.3 and this results in an additional standard deviation of approximately 2.8 for the t-distribution (see section 2.4 for details).

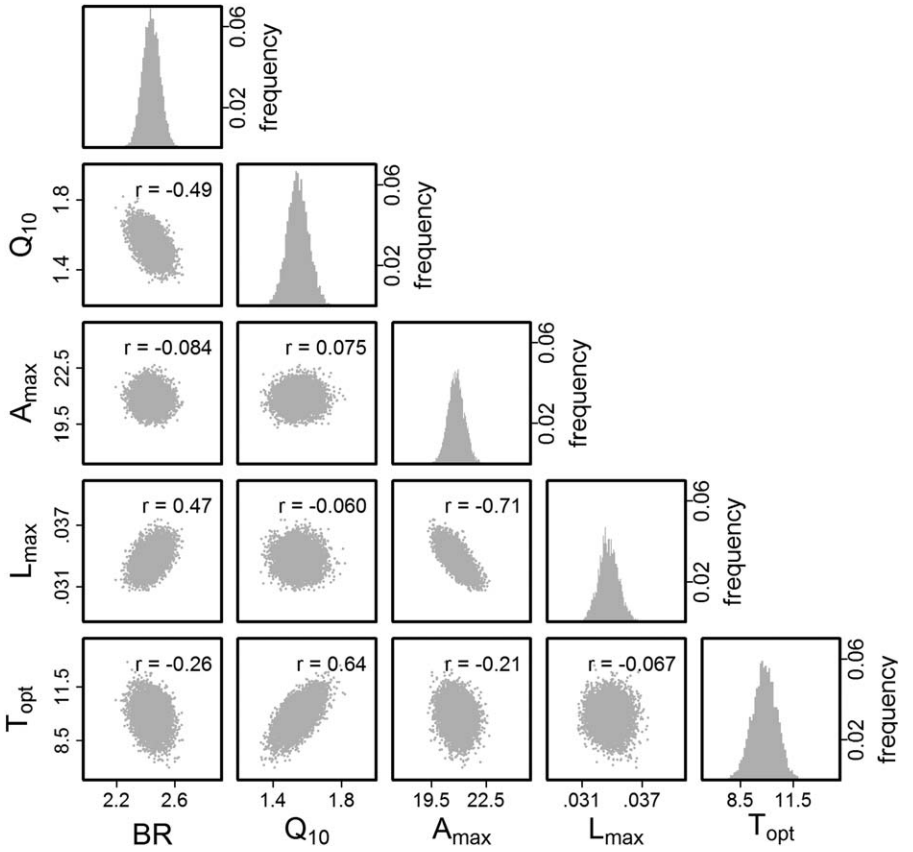

Figure 5. Pairwise scatter plots and histograms of the parameter samples from the posterior. The results are shown for the model based on the t-distribution and restricted to the biophysical parameters, i.e. the estimated nuisance parameters are not shown. The values in the subplots are the correlation coefficients after Pearson (r), parameter description is given in the text. *BR* (μmol m^{-2} s^{-1}) is the base rate respiration at 10°C, Q_{10} is a parameter describing temperature sensitivity, A_{max} (μmol m^{-2} s^{-1}) is the maximum assimilation rate of CO_2, T_{opt} (°C) is the optimal temperature at which the light use efficiency function equals L_{max} (μmol CO2 (μmol PPFD)$^{-1}$), which is the maximum light use efficiency.

Figure 6 shows the marginal posterior distributions of the biophysical model parameters for the different likelihood models. In most cases there is only a (very) small overlap between the marginal distributions obtained using the Gaussian likelihood and the ones compared to using the Laplace or Student's t likelihoods. The latter two have similar spread (variance) and show only slight differences in their modes. The related statistical metrics are provided in Tab. 4.

In addition to the uniqueness of individual parameters dealt with in Figure 6, the uniqueness of the biophysical response functions is illustrated in Figure 7. The functions and their 95%-IQR were obtained by propagating the sample from the posterior parameter pdf through equations (3–5). The study of the response functions reveals that both *GPP* and *ER* will be influenced by the choice of the likelihood function because a switch from the Gaussian to the more dispersed distributions changes all three response functions shown in Figure 7, and closely reflect the discussion of the individual parameters above. The response functions obtained in the case of the normal distribution differ markedly from those obtained for the Laplace and t-distribution, in particular for *ER*. In agreement with Table 4, parameter uncertainty is highest for the Gauss distribution and decreases markedly for the non-Gaussian distributions which show similar 95%-IQR_{par}.

3.4. Time Series of NEE and Model Adequacy

For the sake of brevity, the presentation in this section is restricted to the model calibration using the t-distribution which was shown above to lead to the best statistical description of the error. With a small

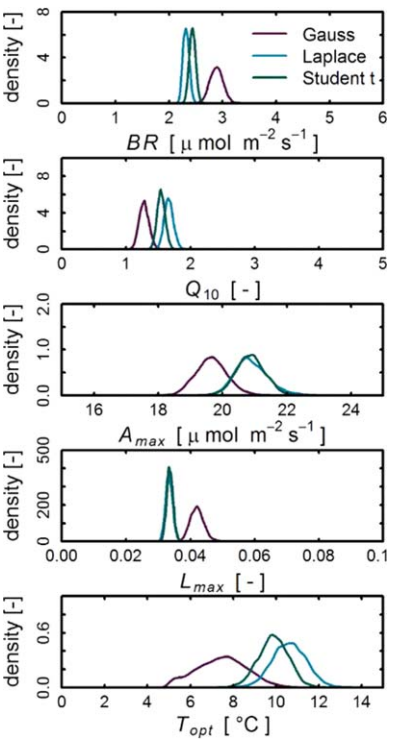

Figure 6. Marginal posterior distributions of the estimated biophysical model parameters for three different statistical models of the error distribution. Parameter description is given in the text. *BR* (μmol m^{-2} s^{-1}) is the base rate respiration at 10°C, Q_{10} is a parameter describing temperature sensitivity, A_{max} (μmol m^{-2} s^{-1}) is the maximum assimilation rate of CO_2, T_{opt} (°C) is the optimal temperature at which the light use efficiency function equals L_{max} (μmol CO_2 (μmol PPFD)$^{-1}$), which is the maximum light use efficiency.

mean weighted error of −0.09 μmol m^{-2} s^{-1} (Table 3), the simulated *NEE* shows a minimal mean deviation from the measured values. In Figure 8a a selected measurement period spanning DOY 190–210 illustrates the excellent model description of the measured *NEE* data. The selected time period is the one with the smallest measured water content, which was selected for two reasons i) it shows contrasting model performances, ii) it contains periods with minimal and maximal prediction intervals, iii) it covers the driest periods (Figure 2) and is; thus, diagnostic for the model performance during these meteorological conditions. The results highlight the feasibility to use a biophysical process model for gap filling, providing the environmental drivers are available and adequately represented in the model. The uncertainty intervals reflecting the uncertainty in the model parameters (IQR_{par}) are very narrow and are almost entirely masked by the line denoting the simulation. Only very few data points lie outside the prediction interval (IQR_{pred}) which represents the uncertainty to observe a single data point. The 95%-prediction intervals have an average width of about 10 μmol m^{-2} s^{-1} and the width closely follows the time series of the D_v. One period during which IQR_{pred} increases is highlighted in Figure 8b (DOY 192). During the early hours, D_v is close to zero and due to the parametrization of heteroscedasticity (equation (10) and parameter values in Table 4), the prediction interval is wide during the morning hours. As the daylight hours begin, D_v increases, the standard deviation of the measurement error decreases and the prediction interval shrinks. Figure 8b also nicely illustrates the influence of $K\downarrow$ on the measured and simulated *NEE* data. During the late morning hours, $K\downarrow$ decreases due to increased cloudiness and both the measurements and the simulations reflect this reduction in supply of energy by a reduced *GPP*. This reaction of the ecosystems response to the environmental driver $K\downarrow$ is reflected in the measurements and model and contributes to the above mentioned minimal autocorrelation in the residuals. Finally, Figure 8c gives an overview of ideal measurement conditions with a sufficiently high D_v (DOY 200) and shows that the observations are described very well by the model which was calibrated over the entire measurement period from June to October.

First we direct the reader to Figure 9, before we finish discussing the results in Figure 8 at the end of this section. Figure 9 shows median daily time series of *NEE* for the individual months June to October and the entire measurement period (bottom, right) and compares measured and calibrated fluxes. The measured and simulated fluxes are very well described from Jun-Oct. Visibly; the individual months are still within good agreement when comparing observed and modelled values, but the match is no longer as exceptional as for the entire period. An explanation can be found through the formulation of Bayes' theorem (equation. (6)) which states that the posterior distribution of the model parameters is conditional on the observed time series of measured CO_2 fluxes. This means the best parameter set is the best estimate conditional to the entire data set, and not automatically for each individual subset. However, we purposefully inverted the entire time series, since a larger environmental variability (presented in Figure 2) and therefore more information is contained in the entire data set, leading to more robust modelling. Clearly, this result shows that for the data set of this peatland and season, which contained a large variability of environmental drivers, monthly estimates of model parameters are not required. Since the monthly subsets are still predicted very well (Figure 9) this is an indication on the robustness of the process model, too. Eco-physiologically, this means that the Odersprungmoor, as an ecosystem, assimilates and releases carbon which can be modelled without additionally accounting for growth and senescence terms as is common in e.g., agro-ecosystems (as indicated in section 3.2). As the ecosystem is not changing its internal features despite the historically extreme dry periods, the model parameters can be treated as constant in time.

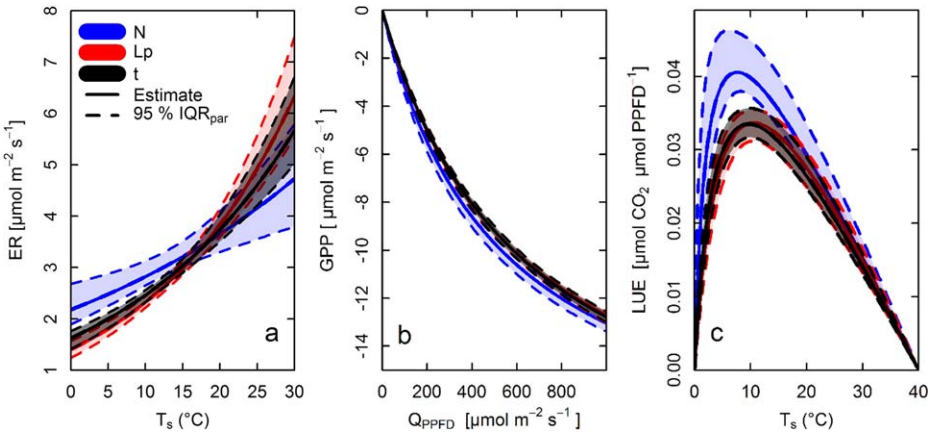

Figure 7. Estimated biophysical response functions and their 95%-IQR for the three different statistical models: a) ecosystem respiration, b) gross primary productivity using the estimated (mode of posterior) L_{max}, and c) the light use efficiency function. T_s (°C) is the soil temperature, Q_{PPFD} (µmol m^{-2} s^{-1}) is the photosynthetically active photon flux density, and L_{max} (µmol CO_2 (µmol PPFD)$^{-1}$) which is the maximum light use efficiency.

The only time period in which a slightly more pronounced mismatch is observable can be found between 7 and 12 am in September. In this period, *GPP* might be underestimated due to a misrepresentation of the T_a-dependent variation of *LUE* in the transition season of the vegetation. Additionally, the night time respiration in July and August is very slightly underestimated.

In the light of the above mentioned results, we wish to focus on some more subtle details of Figure 8. First for the daytime CO_2 fluxes. For a number of days peak CO_2 uptake was systematically underestimated (DOY 194–196, 208, 2010); however, for others it was over-estimated (DOY 202–204), and during a number of days the modelled match the observed very well (DOY 190, 192–193, 201, 205–207-208), the median

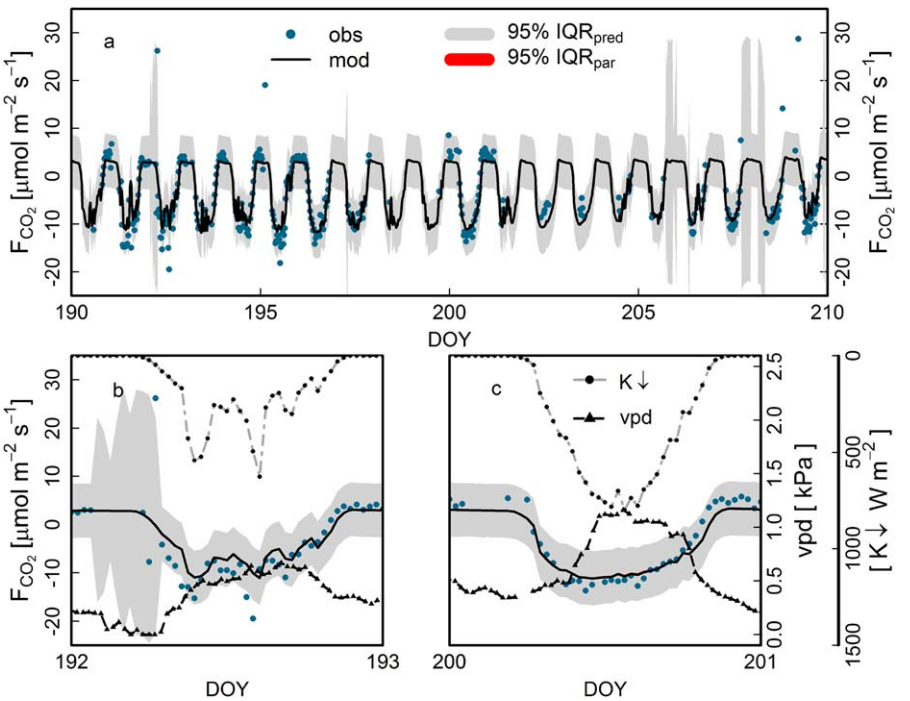

Figure 8. Selected time series of NEE showing measurements, simulations and the 95%-IQR of the model (IQR_{par}) and individual measurements (IQR_{pred}). The IQR_{par} are so narrow that the red lines are not visible. The bottom plots are close-ups highlighting the influence of incoming shortwave radiation (K↓) on NEE and the influence of the VPD on the error standard deviation and thus the width of the prediction interval IQR_{pred}.

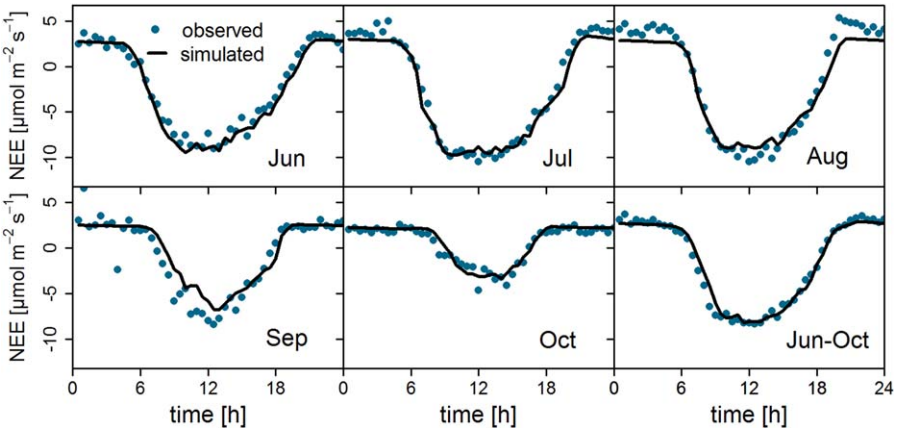

Figure 9. Median daily time series of the measured and simulated NEE for the individual months and the entire measurement period.

daytime fluxes; however, are matched perfectly (Figure 9). For the night-time values, the systematic mismatch appears a little larger, and is also reflected in Figure 9. Since the values for other months are well described during night times (June, September, October), we, as mentioned before, have no explanation for this small difference.

3.5. Net Ecosystem Exchange at the Odersprungmoor

The Odersprungmoor is a mountainous peatland with a small fetch. As a consequence, there are constraints for applying the EC technique and data gaps are both wide and large in number. This makes it difficult to fill the gaps by simple approaches like look-up table methods or mean diurnal variation (Moffat et al., 2007). The well-calibrated biophysical model provides an alternative approach for gap-filling and enables the calculation of the cumulative net ecosystem flux, NEE_{cum} (g C m^{-2}). The NEE_{cum} were −201, −219, and −208 g C m^{-2} for the normal, Laplace and t-distribution, respectively, and the associated widths of the 95%-IQR are 40, 25, and 23 g C m^{-2} (Table 5). In comparison to the model calibration using the normal distribution, the application of the Laplace distribution leads to an increase in carbon uptake of almost 10%. This predicted increase is reduced when switching to the best model, the t-distribution. Although the increase in carbon uptake persists, it amounts to 5% compared to the assumption of Gaussian error. In agreement with the decrease in parameter uncertainty for the Laplace- and t-distributions, the 95%-IQR of the carbon flux decreases markedly when assuming the Laplace- and t-distributions. Overall, accounting for the heavy-tails of the error distribution reduced the width of the uncertainty intervals by a factor of two.

Table 5
Comparison of Cumulative NEE (NEE_{cum}) and the Respective 95%−IQR for the Three Different Statistical Models

	NEE_{cum}	95% CI	NEE_{cum}	95% CI	NEE_{cum}	95% CI
	(g C m^{-2})					
	Normal distribution		Laplace distribution		Student's t distribution	
Jun	−62.8	[−65.6;−59]	−62.7	[−65;−60.6]	−61.5	[−63.6;−59.5]
July	−81.1	[−84.8;−75.8]	−79.5	[−82.8;−76.5]	−78.9	[−81.7;−75.7]
Aug	−59.7	[−63.4;−54.7]	−60.8	[−63.6;−58.1]	−59.0	[−61.8;−56.4]
Sept	−15.3	[−17.9;−10.3]	−20.1	[−22;−17.9]	−17.0	[−19.5;−15.7]
Oct	12.5	[8.9;18.1]	3.59	[1.93;5.75]	7.6	[4.87;8.8]
Jun-Oct	−201	[−182;−222]	−219	[−206;−231]	−208	[198;−221]
Width of 95%-IQR Jun-Oct		40		25		23

Note. Simulations before 7 June are not available.

The highest monthly uptake was determined for July (78.9 g C m^{-2}) and the lowest in October (7.6 g C m^{-2}). The comparison of the different error models underlines the variation of the model output and how it influences monthly modelled NEE_{cum}. In comparison to other micrometeorological studies in peat bogs, the Odersprungmoor assimilated more CO_2 per area than a Swedish eccentric bog (-26.9 g C m^{-2} in June 2006; Lund et al., 2007) or an Irish Atlantic blanket bog (approx. -38 g C m^{-2} in July 2004; Sottocornola & Kiely, 2010). The strong deviation from these bogs could be a result of more favorable climate conditions for plant growth at the Odersprungmoor.

4. Summary and Conclusions

The quantification of the *NEE* of an ombrotrophic bog in a mountainous setting using the EC method and calibration of a common biophysical model, requires assumptions with respect to the statistical distribution of the residuals, i.e. the differences between measured and simulated half-hourly CO_2 fluxes. Different assumptions on the statistical distribution function for the residuals may have far-reaching consequences for the estimated parameters and their uncertainties, but also for the resulting cumulative flux calculations. It has long been noted that classic weighted-least-squares estimation is negatively affected by outliers, i.e. by residuals which are located relatively far away from zero. The Laplace distribution has been discussed as an alternative to least-squares estimation and its influence on statistical inference had been assessed in forest meteorology (Hollinger & Richardson, 2005).

In our study, we compared calculations assuming Gaussian, Laplace and t-distributed residuals. We found that the observed residuals were most accurately described by the Student's t distribution followed by the Laplace distribution. The normal distribution, which is still most frequently applied in model calibration and uncertainty analysis, performed worst in terms of the maximum posterior likelihood and the DIC. Obviously, the ability of the Laplace and t-distributions to model heavier tails of the error distribution led to a better statistical description of the data.

The estimated parameters and the response functions of the biophysical model differed between the three error assumptions. While the difference between the normal distribution and the other two distributions was quite large, the difference between the Laplace and t-distribution was relatively small. A similar conclusion can be drawn for the uncertainty of the estimated parameters and response functions: the uncertainties were highest for the model calibration assuming Gaussian distributed errors, and the uncertainties were reduced when assuming the Laplace and t-distribution by up to 50%, (Table 4). We conclude that the possibility to describe heavier tails of the error distribution reduces estimation uncertainty because it prevents that undue weight is assigned to residuals far away from zero.

The biophysical model was used to fill data gaps and to calculate cumulative C fluxes between the land surface and the atmosphere. For the Odersprungmoor, a C accumulation of -201 g C m^{-2} (+/− 10%) from DOY 158 to DOY 303 was simulated with the calibrated Gaussian model. With the assumption of t-distributed errors, this cumulative flux was -208 g C m^{-2} (+/− 5%). The smaller uncertainties of the estimated parameters obtained for the t-distribution propagated into smaller uncertainties of the model-predicted carbon fluxes. Use of the Laplace error model even led to a 10% higher uptake of -219 g C m^{-2} (+/− 6%). The reduced uncertainties of the estimated parameters obtained for the t-distribution propagated into smaller uncertainties of the model-predicted carbon fluxes. These results illustrate the influence of distributional assumptions on gap-filled cumulative carbon uptake, a highly-relevant issue which requires further investigation.

In addition to an improved statistical model of the error, we introduced an innovative method to parametrize heteroscedasticity into the EC modeling community. For open-path EC systems, heteroscedasticity is caused by the limited precision of the IRGA under conditions of high air humidity. As shown by the analysis of the standardized residuals, this model described heteroscedasticity very well. An important result thereof is that prediction uncertainty can be adequately quantified and that its magnitude varies with varying D_v. We emphasize that the parameters describing heteroscedasticity were included in the estimation as nuisance parameters and have not been specified based on expert knowledge or empirical methods. Summing up, the methodology derived in this study marks an important step towards a better statistical description of EC data with marked effects on calibrated parameters and gap-filled, cumulative NEE.

Future studies should focus on the following issues. Firstly, for a final evaluation of carbon uptake, an extensive monitoring campaign which integrates carbon flux measurements within the soil-plant-atmosphere continuum and aqueous output as possible C pathways has to be implemented for at least a complete year. This would help to assess whether the relatively simple *NEE* model is able to describe fluxes during spring when a complex interplay of environmental factors result in plants starting to be photosynthetically active and during late autumn when vegetation undergoes seasonal senescence. Secondly, as the model was calibrated for one growing season only, it is not possible to extrapolate the ecosystems behavior beyond the observed hydrological and meteorological conditions. Additional seasons worth of measurements from this and other similar peatland sites, can lead to a more rigorous validation of the biophysical model parameterization. Conditions different from this, e.g. during the winter season and under future climate change, require long-term monitoring campaigns. Thirdly, as the EC method can hardly be applied during rain events using open path analyzers, the advective expulsion of CO_2 caused by quick infiltration and fast groundwater rise cannot be captured. Currently, such processes which are only active for limited time periods, are not included in the model formulation. Clearly, such unaccounted processes require further experimental and modeling efforts in the future.

Acknowledgments

We would like to thank Paul Dirmeyer for handling our manuscript. We acknowledge the financial support of the Ministry of Education of the Federal State of Lower Saxony funding the GEOFLUXES top-down-project TD 2.1.4 and the Germany and the German Academic Exchange Service (DAAD) for the scholarship grant to Tobias Weber. Additionally, we wish to extend our gratitude to Jannik Heusinger, Sabrina Martin, and Hagen Mittendorf. Finally, we thank the park authority of the Harz National Park for granting us access to the research site, in particular Dr. Kison. Data is available as Supporting Information, R scripts are available upon request. Thanks to Dr. Arne Poyda, University of Hohenheim for additional comments.

References

Adkinson, A. C., Syed, K. H., & Flanagan, L. B. (2011). Contrasting responses of growing season ecosystem CO2 exchange to variation in temperature and water table depth in two peatlands in northern Alberta, Canada. *Journal of Geophysical Research*, *116*, G01004. https://doi.org/10.1029/2010JG001512

Aster, R. C., Borchers, B., & Thurber, C. H. (2013). *Parameter estimation and inverse problems*. Amsterdam, the Netherlands: Elsevier. https://doi.org/10.1016/B978-0-12-385048-5.00002-1

Batzer, D. P., & Baldwin, A. H. (2012). *Wetland habitats of North America: ecology and conservation concerns*. Berkley: Univ of California Press.

Baumann, K. (2009). *Entwicklung der Moorvegetation im Nationalpark Harz.* [in German]. *In: Schriftenreihe aus dem Nationalpark Harz (Band 4)*, Wernigerode, Germany.

Billesbach, D. P. (2011). Estimating uncertainties in individual eddy covariance flux measurements: A comparison of methods and a proposed new method. *Agricultural and Forest Meteorology*, *151*, 394–405. https://doi.org/10.1016/j.agrformet.2010.12.001

Box, G. E. P., & Tiao, G. C. (1992). Nature of Bayesian Inference. In G. E. P. Box, & G. C. Tiao, Eds., *Bayesian inference in statistical analysis*. (pp. 1–75). Hoboken, NJ: John Wiley & Sons, Inc. https://doi.org/10.1002/9781118033197.ch1

Brooks, S. P. (1998). Markov chain Monte Carlo method and its application. *Journal of Royal Statistical Society D*, *47*, 69–100.

Brown, C., Strack, M., & Price, J. S. (2017). The effects of water management on the CO2 uptake of Sphagnum moss in a reclaimed peatland. *Mires and Peat*, *20*(5), 1–15. https://doi.org/10.19189/MaP.2016.OMB.258

Bubier, J., Crill, P., & Mosedale, A. (2002). Net ecosystem CO2 exchange measured by autochambers during the snow-covered season at a temperate peatland. *Hydrological Processes*, *16*, 3667–3682. https://doi.org/10.1002/hyp.1233

Campbell, D. I., Smith, J., Goodrich, J. P., Wall, A. M., & Schipper, L. A. (2014). Year-round growing conditions explains large CO2 sink strength in a New Zealand raised peat bog. *Agricultural and Forest Meteorology*, *192–193*, 59–68. https://doi.org/10.1016/j.agrformet.2014.03.003

Chen, C., & Mangasarian, O. L. (1996). A class of smoothing functions for nonlinear and mixed complementarity problems. *Computational and Optimization Applications*, *5*(2), 97–138. https://doi.org/10.1007/BF00249052

Etzold, S., Buchmann, N., & Eugster, W. (2010). Contribution of advection to the carbon budget measured by eddy covariance at a steep mountain slope forest in Switzerland. *Biogeosciences*, *7*, 2461–2475. https://doi.org/10.5194/bg-7-2461-2010

Falge, E., Baldocchi, D., Olson, R., Anthoni, P., Aubinet, M., Bernhofer, C., et al. (2001). Gap filling strategies for defensible annual sums of net ecosystem exchange. *Agricultural and Forest Meteorology*, *107*, 43–69. https://doi.org/10.1016/S0168-1923(00)00225-2

Finsterle, S., & Najita, J. (1998). Robust estimation of hydrogeologic model parameters. *Water Resources Research*, *34*, 2939–2947. https://doi.org/10.1029/98WR02174

Foken, T. (2006). *Angewandte Meteorologie [in German]*. Berlin, Germany: Springer. https://doi.org/10.1007/978-3-540-38204-1

Gelman, A., Carlin, J. B., Stein, H. S., & Rubin, D. B. (2004). *Bayesian data analysis*. Boca Raton, FL: Chapman & Hall.

Gilmanov, T. G., Wylie, B. K., Tieszen, L. L., Meyers, T. P., Baron, V. S., Bernacchi, C. J., et al. (2013). CO2 uptake and ecophysiological parameters of the grain crops of midcontinent North America: Estimates from flux tower measurements. *Agriculture, Ecosystems, & Environment*, *164*, 162–175. https://doi.org/10.1016/j.agee.2012.09.017

Gitay, H., Brown, S., Easterling, W., & Jallow, B. (2001). *E*cosystems and their goods and services. In J. J. McCarthy, O. F. Canziani, N. A. Leary, D. J. Dokken, & K. S. White, Eds., *Climate change 2001: Impacts, adaptation, and vulnerability, contribution of working group ii to the third assessment report of the intergovernmental panel on climate change* (pp. 237–342), Cambridge, UK: Cambridge University Press. https://doi.org/10.1387/ijdb.113386mm

Glenn, A. J., Flanagan, L. B., Syed, K. H., & Carlson, P. J. (2006). Comparison of net ecosystem CO2 exchange in two peatlands in western Canada with contrasting dominant vegetation, Sphagnum and Carex. *Agricultural and Forest Meteorology*, *140*, 115–135. https://doi.org/10.1016/j.agrformet.2006.03.020

Gorham, E. (1991). Northern peatlands: Role in the carbon cycle and probable responses to climatic warming. *Ecological Applications*, *1*(2), 182. https://doi.org/10.2307/1941811

Guillaume, F., & Andrews, J. (2012). *dream: DiffeRential evolution adaptive metropolis*. R package version 0.4-2.

Hammerle, A., Haslwanter, A., Schmitt, M., Bahn, M., Tappeiner, U., Cernusca, A., & Wohlfahrt, G. (2007). Eddy covariance measurements of carbon dioxide, latent and sensible energy fluxes above a meadow on a mountain slope. *Boundary-Layer Meteorology*, *122*, 397–416. https://doi.org/10.1007/s10546-006-9109-x

Hattermann, F. F., Weiland, M., Huang, S., Krysanova, V., & Kundzewicz, Z. W. (2011). Model-supported impact assessment for the water sector in Central Germany under climate change––A case study. *Water Resources Management*, *25*, 3113–3134. https://doi.org/10.1007/s11269-011-9848-4

Heusinger, J., & Weber, S. (2017). Surface energy balance of an extensive green roof as quantified by full year eddy-covariance measurements. *Science of the Total Environment*, *577*, 220–230.
Hollinger, D. Y., & Richardson, A. D. (2005). Uncertainty in eddy covariance measurements and its application to physiological models. *Tree Physiology*, *25*, 873–885. https://doi.org/10.1093/treephys/25.7.873
Humphreys, E. R., Lafleur, P. M., Flanagan, L. B., Hedstrom, N., Syed, K. H., Glenn, A. J., & Granger, R. (2006). Summer carbon dioxide and water vapor fluxes across a range of northern peatlands. *Journal of Geophysical Research*, *111*, G04011. https://doi.org/10.1029/2005JG000111
Iden, S. C., & Durner, W. (2008). Multiple batch extraction test to estimate contaminant release parameters using a Bayesian approach. *Journal of Contaminant Hydrology*, *95*(2008), 168–182. https://doi.org/10.1016/j.jconhyd.2007.09.004
Iden, S. C., & Durner, W. (2014). Comment on "Simple consistent models for water retention and hydraulic conductivity in the complete moisture range" by A. Peters. *Water Resources Research*, *50*, 7530–7534. https://doi.org/10.1002/2014WR015937
Jensen, U. (1990). *Die Moore des Hochharzes*. Hannover, Germany: Spezieller Teil. Niedersächsisches Landesverwaltungsamt.
Joseph, J. F., & Guillaume, J. H. A. (2013). Using a parallelized MCMC algorithm in R to identify appropriate likelihood functions for SWAT. *Environmental Modelling & Software*, *46*, 292–298.
Kellner, E. (2001). Surface energy fluxes and control of evapotranspiration from a Swedish Sphagnum mire. *Agricultural and Forest Meteorology*, *110*, 101–123. https://doi.org/10.1016/S0168-1923(01)00283-0
Kljun, N., Calanca, P., Rotach, M. W., & Schmid, H. P. (2004). A simple parameterisation for flux footprint predictions. *Boundary-Layer Meteorology*, *112*, 503–523. https://doi.org/10.1023/B:BOUN.0000030653.71031.96
Kormann, R., & Meixner, F. X. (2001). An analytical footprint model for non-neutral stratification. *Boundary-Layer Meteorology*, *99*, 207–224. https://doi.org/10.1023/A:1018991015119
Kurbatova, J., Arneth, A., Vygodskaya, N. N., Kolle, O., Varlargin, A. V., Milyukova, I. M., et al. (2002). Comparative ecosystem – atmosphere exchange of energy and mass in a European Russian and a central Siberian bog I. Interseasonal and interannual variability of energy and latent heat fluxes during the snowfree period. *Tellus, Series B*, *54*, 497–513. https://doi.org/10.1034/j.1600-0889.2002.01354.x
Lafleur, P. M., Roulet, N. T., & Admiral, S. W. (2001). Annual cycle of CO2 exchange at a bog peatland. *Journal of Geophysical Research*, *106*, 3071–3081. https://doi.org/10.1029/2000JD900588
Lange, K. L., Little, R. J. A., & Taylor, J. M. G. (1989). Robust statistical modeling using the t distribution. *Journal of American Statistical Association*, *84*, 881–896. https://doi.org/10.1080/01621459.1989.10478852
Lasslop, G., Reichstein, M., Kattge, J., & Papale, D. (2008). Influences of observation errors in eddy flux data on inverse model parameter estimation. *Biogeosciences Discussions*, , *5*(1), 751–785. https://doi.org/10.5194/bgd-5-751-2008
Lasslop, G., Reichstein, M., Papale, D., Richardson, A., Arneth, A., Barr, A. et al. (2010). Separation of net ecosystem exchange into assimilation and respiration using a light response curve approach: Critical issues and global evaluation. *Global Chang. Biology*, *16*, 187–208. https://doi.org/10.1111/j.1365-2486.2009.02041.x
Lindroth, A., Lund, M., Nilsson, M., Aurela, M., Christensen, T. R., Laurila, T., et al. (2007). Environmental controls on the CO2 exchange in north European mires. *Tellus, Series B*, *59*, 812–825. https://doi.org/10.1111/j.1600-0889.2007.00310.x
Lund, M., Lindroth, A., Christensen, T. R., & Ström, L. (2007). Annual CO2 balance of a temperate bog. *Tellus B: Chemical and Physical Meteorology*, *59*(5), 804–811. https://doi.org/10.1111/j.1600-0889.2007.00303.x
McCree, K. J. (1972). Test of current definitions of photosynthetically active radiation against leaf photosynthesis data. *Agricultural and Forest Meteorology.*, 10, 443–453. https://doi.org/10.1016/0002-1571(72)90045-3
Moffat, A. M., Papale, D., Reichstein, M., Hollinger, D. Y., Richardson, A. D., Barr, A. G., et al. (2007). Comprehensive comparison of gap-filling techniques for eddy covariance net carbon fluxes. *Agricultural and Forest Meteorology*, *147*, 209–232. https://doi.org/10.1016/j.agrformet.2007.08.011
Moncrieff, J. B., Malhi, Y., & Leuning, R. (1996). The propagation of errors in long-term measurements of land-atmostphere fluxes of cabron and water. *Global Change Biology*, *2*, 231–240.
Moore, T. R., Lafleur, P. M., Poon, D. M. I., Heumann, B. W., Seaquist, J. W., & Roulet, N. T. (2006). Spring photosynthesis in a cool temperate bog. *Global Change Biology*, *12*, 2323–2335. https://doi.org/10.1111/j.1365-2486.2006.01247.x
Nicolini, G., Fratini, G., Avilov, V., Kurbatova, J. A., Vasenev, I., & Valentini, R. (2015). Performance of eddy-covariance measurements in fetch-limited applications. *Theoretical and Applied Climatology*, 829–840. https://doi.org/10.1007/s00704-015-1673-x
Parmentier, F. J. W., van der Molen, M. K., de Jeu, R. A. M., Hendriks, D. M. D., & Dolman, A. J. (2009). CO2 fluxes and evaporation on a peatland in the Netherlands appear not affected by water table fluctuations. *Agricultural and Forest Meteorology*, *149*, 1201–1208. https://doi.org/10.1016/j.agrformet.2008.11.007
Pullens, J., Sottocornola, M., Kiely, G., Toscano, P., & Gianelle, D. (2016). Carbon fluxes of an alpine peatland in Northern Italy. *Agricultural and Forest Meteorology*, *220*, 69–82. https://doi.org/10.1016/j.agrformet.2016.01.012
R Core Team. (2015). *R: A language and environment for statistical computing*. Vienna Austria: R Found. Stat. Comput. ISBN 3–900051-07-0.
Raj, R., Hamm, N. A. S., van der Tol, C., & Stein, A. (2016). Uncertainty analysis of gross primary production partitioned from net ecosystem exchange measurements. *Biogeosciences*, *13*, 1309–1422. https://doi.org/10.5194/bgd-12-13967-2015
Reichert, P., & Omlin, M. (1997). On the usefulness of overparameterized ecological models. *Ecological Modelling*, *95*, 289–299. https://doi.org/10.1016/S0304-3800(96)00043-9
Richardson, A. D., Mahecha, M. D., Falge, E., Kattge, J., Moffat, A. M., Papale, D., et al. (2008). Statistical properties of random CO 2 flux measurement uncertainty inferred from model residuals. *Agricultural and Forest Meteorology*, *148*, 38–50. https://doi.org/10.1016/j.agrformet.2007.09.001
Runkle, B. R. K., Wille, C., Gažovič, M., Wilmking, M., & Kutzbach, L. (2014). The surface energy balance and its drivers in a boreal peatland fen of northwestern Russia. *Journal of Hydrology*, *511*, 359–373. https://doi.org/10.1016/j.jhydrol.2014.01.056
Scharnagl, B., Iden, S. C., Durner, W., Vereecken, H., & Herbst, M. (2015). Inverse modelling of in situ soil water dynamics: Accounting for heteroscedastic, autocorrelated, and non-Gaussian distributed residuals. *Hydrology and Earth System Science Discussions*, *12*, 2155–2199. https://doi.org/10.5194/hessd-12-2155-2015
Serrano-Ortiz, P., Kowalski, A. S., Domingo, F., Ruiz, B., & Alados-Arboledas, L. (2008). Consequences of Uncertainties in CO_2 density for estimating net ecosystem CO_2 exchange by open-path Eddy covariance. *Boundary-Layer Meteorology*, *126*, 209–218. https://doi.org/10.1007/s10546-007-9234-1
Sottocornola, M., & Kiely, G. (2010). Hydro-meteorological controls on the CO2 exchange variation in an Irish blanket bog. *Agricultural and Forest Meteorology*, *150*, 287–297. https://doi.org/10.1016/j.agrformet.2009.11.013
Spiegelhalter, D. J., Best, N. G., Carlin, B. P., & Linde, A. V D. (2002). Bayesian measures of model complexity and fit (with discussion). *Journal of Royal Statistical Society B*, *64*, 583–639.
Stiperski, I., & Rotach, M. W. (2016). On the measurement of turbulence over complex mountainous terrain. *Boundary-Layer Meteorology*, *159*, 97–121. https://doi.org/10.1007/s10546-015-0115-8

Strachan, I. B., Pelletier, L., & Bonneville, M.-C. M.-C. (2016). Inter-annual variability in water table depth controls net ecosystem carbon dioxide exchange in a boreal bog. *Biogeochemistry*, *127*, 99–111. https://doi.org/10.1007/s10533-015-0170-8

Strack, M., Keith, A. M., & Xu, B. (2014). Growing season carbon dioxide and methane exchange at a restored peatland on the Western Boreal Plain. *Ecological Engineering*, *64* (2014), 231–239.

Strack, M., & Zuback, Y. C. A. (2013). nnual carbon balance of a peatland 10 yr following restoration. *Biogeosciences*, *10*, 2885–2896.

Sutherland, G., Chasmer, L. E., Petrone, R. M., Kljun, N., & Devito, K. J. (2014). Evaluating the use of spatially varying versus bulk average 3D vegetation structural inputs to modelled evapotranspiration within heterogeneous land cover types. *Ecohydrology.*, *7*(6), 1545–1559. https://doi.org/10.1002/eco.1477

Szeicz, G. (1974). Solar radiation for plant growth. *Journal of Applied Ecology*, *11*(2), 617–636.

Tamiya, H. (1951). Some theoretical notes on the kinetics of algal growth. *The Botanical Magazine*, *64*, 167–173.

Van't Hoff, J. H. (1898). *Lectures on theoretical and physical chemistry. Part I. Chemical dynamics* (translated by R. A. Lehfeldt). London, UK: Edward Arnold.

Van Wijk, M. T., van Putten, B., Hollinger, D. Y., & Richardson, A. D. (2008). Comparison of different objective functions for parameterization of simple respiration models. *Journal of Geophysical Research*, *113*, G03008. https://doi.org/10.1029/2007JG000643

Vrugt, J. A. (2016). Markov chain Monte Carlo simulation using the DREAM software package: Theory, concepts, and MATLAB Implementation. *Environmental Modeling & Software*, *75*, 273–316. https://doi.org/10.1016/j.envsoft.2015.08.013

Vrugt, J. A., ter Braak, C. J. F., Gupta, H. V., & Robinson, B. A. (2009). Equifinality of formal (DREAM) and informal (GLUE) Bayesian approaches in hydrologic modeling?. *Stochastic Environmental Research and Risk Assessment*, *23*, 1011–1026. https://doi.org/10.1007/s00477-008-0274-y

Weber, S., & Kordowski, K. (2010). Comparison of atmospheric turbulence characteristics and turbulent fluxes from two urban sites in Essen, Germany. *Theoretical and Applied Climatology*, *102*, 61–74.

Weber, T. K. D., Iden, S. C., & Durner, W. (2017a). Unsaturated hydraulic properties of Sphagnum moss and peat reveal trimodal pore-size distributions. *Water Resources Research*, *53*, 415–434. https://doi.org/10.1002/2016WR019707

Weber, T. K. D., Iden, S. C., & Durner, W. (2017b). A pore-size classification for peat bogs derived from unsaturated hydraulic properties. *Hydrology and Earth System Sciences*, *21*(12), 6185–6200. https://doi.org/10.5194/hess-21-6185-2017

Yuan, W., Liu, S., Zhou, G., Zhou, G., Tieszen, L. L., Baldocchi, D., et al. (2007). Deriving a light use efficiency model from eddy covariance flux data for predicting daily gross primary production across biomes. *Agricultural and Forest Meteorology*, *143*, 189–207. https://doi.org/10.1016/j.agrformet.2006.12.001

Zobitz, J. M., Desai, A. R., Moore, D. J. P., & Chadwick, M. A. (2011). A primer for data assimilation with ecological models using Markov Chain Monte Carlo (MCMC). *Oecologia*, *167*, 599–611. https://doi.org/10.1007/s00442-011-2107-9